

Application of interval field method to the stability analysis of slopes in presence of uncertainties

Chengxin Feng^{a,*}, Matthias Faes^b, Matteo Broggi^a, Chao Dang^a, Jiashu Yang^{a,e}, Zhibao Zheng^c, Michael Beer^{a,d,e,f}

^a*Institute for Risk and Reliability, Leibniz University Hannover, Callinstr. 34, 30167 Hannover, Germany*

^b*TU Dortmund University, Chair for Reliability Engineering, Leonhard-Euler-Strasse 5, 44227 Dortmund.*

^c*Institute of Mechanics and Computational Mechanics, Leibniz University Hannover, Appelstraße 9a, 30167 Hannover, Germany*

^d*Institute for Risk and Uncertainty and School of Engineering, University of Liverpool, Liverpool L69 7ZF, UK*

^e*International Joint Research Center for Engineering Reliability and Stochastic Mechanics, Tongji University, Shanghai 200092, PR China*

^f*International Joint Research Center for Resilient Infrastructure, Tongji University, Shanghai 200092, PR China*

Abstract

Spatial uncertainty of soil parameters has a significant impact on the analysis of slope stability. Interval field analysis is emerging as a complementary tool of the conventional random field method that can take spatial uncertainty into account, which, however, has not been investigated in slope stability analysis. The present paper proposes a new method, named the interval field limit equilibrium method (IFLEM), for assessing the stability of slope in the presence of the interval field. In this method, the modified exponential function is introduced to characterize the spatial uncertainty of the interval field and the Karhunen-Loève-like decomposition is employed to generate the interval field. Then, in a single calculation, the deterministic slope stability analyzed by the Morgenstern-Price approach is implemented in order to estimate the safety factor. Subsequently, the upper and lower bounds of the interval of safety factor are efficiently evaluated by a kind of surrogate-assisted global optimization algorithms, such as Bayesian global optimization used in this study. Finally, the effectiveness of the proposed method is verified by three numerical examples. The results indicate that the proposed method can provide reasonable accuracy and efficiency, which is potentially applicable to a number of geotechnical systems.

Keywords: Spatial uncertainty, Interval field, Spatial dependency function, Karhunen-Loève like expansion, Slope stability

1. Introduction

Slope failure is a major threat to people's lives and property in mountainous areas. Due to the complex material composition and various deposition conditions, there is considerable spatial uncertainty in the properties of geotechnical materials (Phoon and Kulhawy, 1999a). Previous studies have indicated that the spatial uncertainty usually has a great impact on the design and analysis of geotechnical structures, hence it should be properly taken into account (Lämsivaara et al., 2021). The random field theory as one of the feasible techniques to characterize the spatial uncertainty (Phoon and Kulhawy, 1999b; Griffiths and Fenton, 2004). A series of progresses have been emerged in recent decades, particularly a comprehensive overview is given (Jiang et al., 2022). Although the random field theory can address the spatial uncertainties, it requires a large number of samples to obtain statistical characteristics, such as mean value, coefficient of variation, and correlation function. However, it is difficult to estimate these parameters in the presence of sparse measurement data, particularly the correlation length and correlation function (Cami et al., 2020). To address the challenges connected to the statistical inference of the properties of autocorrelation functions, Wang et al. (2019) proposed a bootstrap method for statistically inferring the autocorrelation coefficients as well other parameters of a random field. However, for sparsely sampled random fields, extra statistical uncertainties are introduced when estimating the sampling distribution of the random field parameters (Montoya-Noguera et al., 2019).

Alternatively to random fields, the interval field method proposed by Moens et al. (2011) only requires the upper and lower bounds of material parameters, as well as a description of the spatial dependence for modelling the spatial information. As a possibilistic method, the interval field method has rapidly developed in recent years, and a large number of studies have been conducted to compare it with probabilistic random fields. For instance, Chen et al. (2020) made an objective comparison between the interval and random field methods for the modelling of spatial uncertainty in the case of sparse data. The researchers have shown that the interval field method and the random field method are not competing but complementary. This complementarity was earlier illustrated by Elishakoff et al. (1994), who compared structural models with initial imperfections via stochastic and nonstochastic models and concluded that if probabilistic information

55 is available, one has to use a probabilistic approach and if the probabilistic information is unavailable, one
56 should use nonstochastic approach for uncertainty quantification. The characteristics of interval fields are
57 particularly desirable in cases where statistical data are lacking (Beer et al., 2013; Faes and Moens, 2019).
58 This method represents the uncertainty of bounded parameters that vary in time or space as a series of
59 deterministic basis functions multiplied by a superposition of interval factors. So far, a number of scholars
60 have promoted the interval field method in different fields. Faes and Moens (2017, 2020a) presented a novel
61 methodology for the identification and quantification of spatial uncertainty modelled as an interval field,
62 including potential cross-dependence. Sofi et al. (2015, 2019) introduced an interval finite element method
63 which incorporates the interval field representation of uncertainties by applying an interval extension in
64 conjunction with the standard energy approach. Ni and Jiang (2020) proposed an interval field model to
65 represent spatial uncertainties with insufficient information, in which the variation of the parameters at each
66 location is quantified by an interval with upper and lower bounds. Callens et al. (2021) presented a method
67 to model local explicit interval fields, which are less computationally demanding and less conservative than
68 global explicit interval fields. From the preceding discussion, it can be seen that the interval field method
69 is receiving growing attention, but its application in geotechnical engineering is rarely reported. Therefore,
70 the present study expands its scope on characterizing the spatial uncertainty in geotechnical engineering.

71 In practical terms, an interval field can be regarded as a family of dependent interval variables indexed
72 by location. When considering this interpretation, the methods developed for propagating interval variables
73 could also be applicable to the propagation of interval fields. Over the past several decades, a plethora of
74 methods have been developed for interval uncertainty propagation, such as the interval arithmetic (Moens
75 and Hanss, 2011), the interval perturbation methods (Wang et al., 2014) and the global optimization ap-
76 proach (Deng et al., 2017), etc. It is recommended to refer to (Faes and Moens, 2020b) for a comprehensive
77 review on the related computational methods. Among these algorithms, global optimization approaches are
78 the standard technique for solving interval problems. The main downside is the computational effort of these
79 approaches. To reduce the computational efforts required by heuristic global optimization algorithms (e.g.,
80 genetic algorithm), Kriging-assisted global optimization techniques have been investigated in the context of

81 interval uncertainty propagation (Catallo, 2004). In this direction, a Bayesian global optimization is also
82 presented to obtain the lower and upper response bounds of a computationally expensive model subject to
83 multiple interval variables (Dang et al., 2022).

84 In this paper, the stability analysis of slopes is analyzed when the spatial uncertainty affecting the slopes
85 is modeled by interval fields. The main contributions of this work are summarized as follows: first, the
86 interval field is introduced to characterize the spatial uncertainty of slopes. This is a modelling strategy
87 complementary to the conventionally used random fields, and it is, to the authors' best knowledge, applied
88 to slope stability for the first time. In this representation, an expansion over an orthogonal basis, similar
89 to the Karhunen-Loève-like decomposition in random field analysis, is used to represent the interval field
90 by employing multiple interval variables. Second, a general methodology, called the interval field limit equi-
91 librium method (IFLEM), is proposed to propagate interval fields in slopes. This approach estimates the
92 resulting lower and upper bounds of the safety factor of the slope stability. Additionally, the Bayesian global
93 optimization algorithm is applied to find the lower and upper bounds of the safety factor of a slope char-
94 acterized by multiple interval variables, where the Morgenstern-Price method is employed for deterministic
95 analysis.

96 The rest of this paper is arranged as follows: section 2 introduces the basic knowledge of the interval
97 field, and section 3 incorporates the methodology that will be used in this paper. Section 4 illustrates the
98 procedure of the interval field limit equilibrium method. Three numerical examples are given to demonstrate
99 the effectiveness of the interval field limit equilibrium method in section 5, and conclusions are drawn in
100 section 6.

101 2. Interval field theory

102 An interval field can be understood as a set of dependent intervals indexed by the location through-
103 out the model domain and/or time. The interval field model solves the problems of changing mechanical
104 parameters with spatial location from a non-probabilistic perspective by measuring the spatial uncertainty
105 of the parameters in the form of upper and lower bounds (Sofi et al., 2019). Specifically, the represent

106 interval fields are based on spatial dependence functions and Karhunen-Loève (K-L) like expansions. The
 107 spatial dependence function is adopted to represent the dependence of interval variables in different spatial
 108 positions. In addition, the specific expansion form of the interval fields can be obtained through the K-L
 109 like series expansion.

110 2.1. Interval field expansion

111 In probability theory, random fields are generally used to quantify the uncertainty of a spatially uncertain
 112 parameter, in which the quantity at arbitrary location $\mathbf{x} \in \Omega \subset \mathbb{R}^{n_d}$ is considered as a random variable with
 113 a probability distribution, where \mathbf{x} is the spatial coordinate in n_d dimensions in the physical model domain
 114 Ω . Different from the random field model, the interval field model employs bounds, namely a pair of upper
 115 and lower bounds, to describe the spatial uncertainty, which can efficiently perform uncertainty analysis
 116 based on limited information (Chen et al., 2020). For specific problems, how to represent the interval field
 117 is the basis of simulation calculations. In this paper, the K-L like expansion is used to represent the interval
 118 field $\psi^I(\mathbf{x}) : \Omega \times \mathbb{I}\mathbb{R} \mapsto \mathbb{I}\mathbb{R}$, with $\mathbb{I}\mathbb{R}$ the space of interval valued real numbers. The expansion of an interval
 119 field is written as:

$$\psi^I(\mathbf{x}) = \psi_o^I(1 + \psi_n^I(\mathbf{x})), \quad (1)$$

$$\psi_n^I(\mathbf{x}) = \sum_{j=1}^{\infty} \sqrt{\lambda_j} f_j(\mathbf{x}) \zeta_j, \quad (2)$$

121 where ψ_o^I is the center value of the interval field, $\psi_n^I(\mathbf{x})$ is a dimensionless interval field with unit range,
 122 $\lambda_m \in [0, \infty)$ is the m -th eigenvalue of the spatial dependency function, $f_m : \Omega \mapsto \mathbb{R}$ is the m -th eigenfunction
 123 of the spatial dependency function, and $\zeta_j \in \mathbb{I}\mathbb{R}$ is the j -th extra unitary interval (Sofi, 2015).

124 The extra unitary interval is quite different from the classical unitary interval. It relies on the rules of
 125 the classical interval analysis. The specific details about the classical interval analysis can be found in (Sofi,
 126 2015). The extra unitary interval is given by

$$\zeta_j \in [-1, 1], \quad j = 1, 2, \dots, l. \quad (3)$$

127 Besides, the uncertain flexibility of the spatial dependency condition is described by a single interval
 128 variable constant over the whole range (Sofi, 2015). For that, the following equality holds

$$\zeta_j \times \zeta_j = [0, 1]. \quad (4)$$

129 For numerical implementation, the interval field is represented by l -term expansions. To be specific, the
 130 l -term expansions of the interval field reads

$$\psi^I(\mathbf{x}) = \psi_o^I \left(1 + \sum_{j=1}^l \sqrt{\lambda_j} f_j(\mathbf{x}) \zeta_j \right). \quad (5)$$

131 For details of the method, the reader is referred to the work of Sofi et al. (2019). In this process, the
 132 error of the l -term expansions of the interval field can be represented as:

$$\varepsilon_t(\psi^I(\mathbf{x})) = 1 - \frac{\sum_{j=1}^l \lambda_j}{\sum_{j=1}^{\infty} \lambda_j}, \quad (6)$$

133 where $\varepsilon_t \in [0, \infty)$ is the error of the l -term expansions of the interval field, λ_j is j -th eigenvalue.

134 2.2. Spatial dependency function

135 In essence, each realization of an interval field may vary arbitrarily within the upper and lower bounds,
 136 due to the by-definition orthogonality of intervals. This might lead to spurious, non-physical results. To
 137 overcome this shortcoming, a dependency function needs to be introduced to provide a set of basis functions
 138 upon which the orthogonal intervals can be projected. The key idea behind the interval field model is to
 139 describe the spatial dependency of the uncertain property by introducing a real, deterministic, symmet-
 140 ric, non-negative function $\gamma(\mu, \nu)$. This function is known as the spatial dependency function Sofi et al.
 141 (2019). Specifically, the spatial dependence function provides a method to measure the dependence be-
 142 tween dimensionless interval functions at different locations, effectively providing us with a tool to model
 143 spatially dependent intervals. In analogy with the auto-correlation function characterizing a random field,
 144 the analytic expression of $\gamma(\mu, \nu)$ needs to be assumed in a consistent way with the engineering information
 145 (Sofi, 2015). Alternatively, it can also be fitted onto data, for instance using the methodologies reported
 146 in Faes and Moens (2017) or Ni and Jiang (2020). Application of a dependency function ensures that the

147 realisations of the interval field, as sketched in Fig. 1, are physically realistic. In this figure, we assumed
 148 for simplicity that the upper and lower bounds are constant. The function $\gamma(\mu, v)$ reflects the dependency
 149 between values of the interval field at different locations.

150 In this paper, the $\gamma(\mu, v)$ is used to characterize spatial uncertainty and has a number of formulations,
 151 such as the single exponential model, squared exponential model, etc (Cami et al., 2020). Among them, the
 152 modified exponential model is differentiable at the origin, such that the K-L expansion itself exhibits higher
 153 computational efficiency (Spanos et al., 2007; Faes et al., 2022). Thus, in this paper, we assumed that the
 154 spatial dependency function, $\gamma(\mu, \mu', v, v')$, has the following modified exponential form:

$$\gamma(\mu, \mu', v, v') = \exp\left(-\frac{|\mu - \mu'|}{l_h} - \frac{|v - v'|}{l_v}\right) \left(1 + \frac{|\mu - \mu'|}{l_h}\right) \left(1 + \frac{|v - v'|}{l_v}\right), \quad (7)$$

155 where $\gamma(\mu, \mu', v, v')$ is the spatial dependency function, (μ, v) and (μ', v') denote two points in a 2-D space,
 156 $\exp(\cdot)$ is the exponential function, l_h is the horizontal spatial dependency length which is similar to the
 157 horizontal correlation distance, l_v is the vertical spatial dependency length which is similar to the vertical
 158 correlation distance, $|\mu - \mu'|$ and $|v - v'|$ respectively denote the horizontal and vertical distances between
 159 the two points.

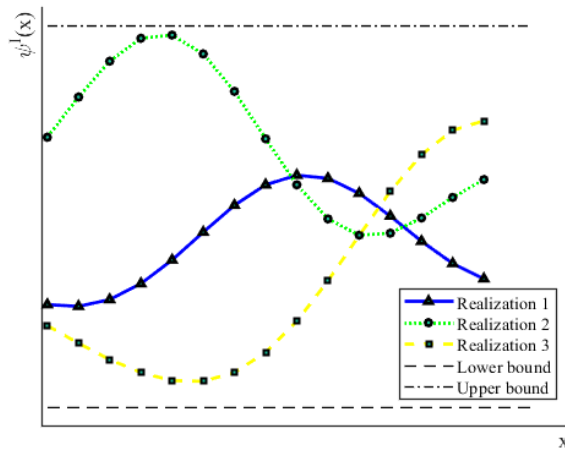


Fig. 1. Sketch of the interval field

160 In this paper, an assumed spatial dependency function, the modified exponential function is used for

161 illustrative purpose. After the spatial dependency function $\gamma(\mu, \mu', v, v') : \Omega \times \Omega \mapsto \mathbb{R}$ is determined, the
 162 spatial uncertainty can then be characterized (Faes et al., 2022). Specifically, the Fredholm integral equation
 163 of the second kind is solved to obtain the eigenvalues and eigenfunctions of the $\gamma(\mu, \mu', v, v')$ (Atkinson and
 164 Han, 2009). The Fredholm integral equation of the second kind takes the form:

$$\int_{\Omega} \gamma(\mu, \mu', v, v') f_j(\mu', v') d\mu' dv' = \lambda_j f_j(\mu, v), \quad (8)$$

165 where λ_j is the j -th eigenvalue of the spatial dependency function, and $f_j(\cdot)$ is the j -th eigenfunction of
 166 the spatial dependency function. In order to numerically solve the Fredholm integral equation of the second
 167 kind, the interval field is first discretized into a series of points, and the integral Eq. (8) is solved by
 168 determining the eigenvalues and eigenvectors of the covariance matrix.

169 3. Interval field limit equilibrium method

170 In this section, the fundamental knowledge and computational formula of the proposed interval field
 171 limit equilibrium method are introduced. First, a limit equilibrium method, namely the Morgenstern-Price
 172 method, is introduced to calculate the safety factor of the slope with the interval field of cohesion and
 173 internal friction angle. Then, the Bayesian global optimization is elaborated to calculate the upper and
 174 lower bounds of the safety factor of this slope.

175 3.1. Limit equilibrium method and its extension to interval field

176 Soil slope stability analysis refers to the analysis of the mutual balance between sliding factors and
 177 resistance factors on the sliding surface of a soil slope. Soil slope has the tendency to move downward and
 178 outward under the action of gravity and other external forces, if the soil inside the slope can resist this
 179 tendency, then the slope is stable, otherwise sliding will occur (Liu et al., 2015).

180 The limit equilibrium method (LEM) used in this paper is the Morgenstern-Price method. The Morgenstern-
 181 Price method is similar to the Spencer method, but it allows for various user-specified interslice force func-
 182 tions (Morgenstern and Price, 1965). In the Morgenstern-Price method, it is assumed that

$$\chi_1/e_1 = \tan \beta = \lambda f(u), \quad (9)$$

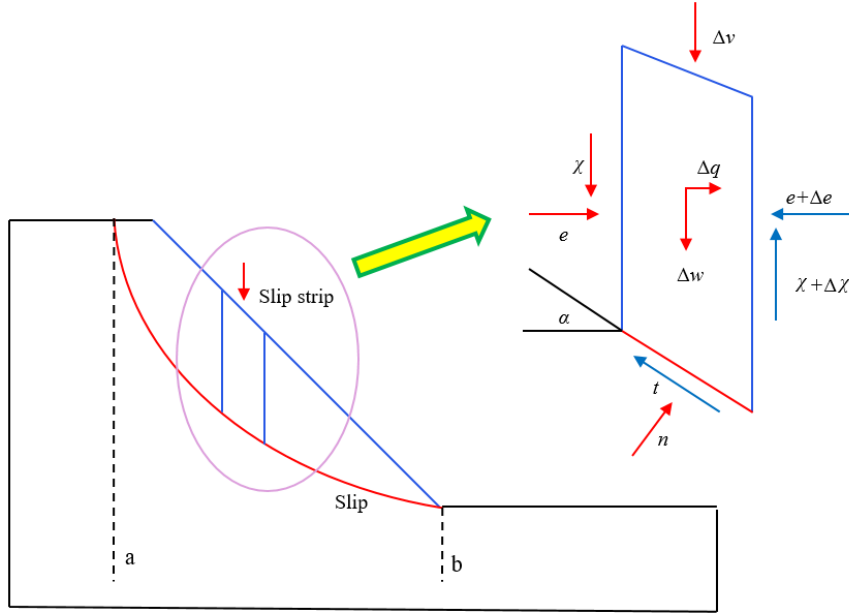


Fig. 2. Schematic diagram of limit equilibrium method

183 where χ_1 is inter-slice vertical force, e_1 is inter-slice horizontal force, λ is a constant, and f is an inter-slice
 184 function. In particular, the inter-slice functions in the present implementation is half-sine function.

185 According to Fig. 2, the equilibrium equations of the forces in the horizontal and vertical directions are
 186 derived respectively. In the process, cohesion and internal friction angle are expressed in the form of interval
 187 fields. The obtained equations are shown as follows:

$$t \sin \alpha + n \cos \alpha = \Delta w + \Delta v - \Delta \chi, \quad (10)$$

188

$$t \cos \alpha - n \sin \alpha = \Delta q - \Delta e, \quad (11)$$

189

$$t \cos \alpha = \psi_c^I \Delta p \sec \alpha + n \tan \psi_\varphi^I, \quad (12)$$

190 where t is tangential force at the bottom of the soil strip, n is the normal force at the bottom of the soil
 191 strip, α is the angle between the tangent line at the bottom of the soil strip and the horizontal direction,
 192 Δw is the gravity of the soil strip, Δv is the external force on the soil strip in the vertical direction, $\Delta \chi$ is

193 the difference in vertical force between strips on both sides of the soil strip, Δq is the horizontal component
 194 of the soil strip, Δe is the difference in horizontal force between strips on both sides of the soil strip, ψ_c^I is
 195 the interval field of c , and ψ_φ^I is the interval field of φ .

196 In addition, the equilibrium equation of the moment is derived as follows

$$(\chi + \Delta\chi) \frac{\Delta p}{2} + \chi \frac{\Delta p}{2} + (e + \Delta e) \Delta q - e \Delta r - \Delta q \Delta s = 0, \quad (13)$$

197 where χ is the lower soil bar which is subjected to the inter-slice vertical force of the upper soil bar, Δp is
 198 the width of the soil strip, e is the lower soil strip is subjected to the horizontal force between the strips of
 199 the upper soil strip, Δq is the distance between the position of the force of the lower soil strip on the upper
 200 soil strip and the center point of the bottom of the strip, Δr is the distance between the position of the
 201 force of the upper soil strip on the lower soil strip and the center point of the bottom of the strip, and Δs is
 202 the distance between the position of the horizontal component of the soil strip and the center of the bottom
 203 of the strip.

204 Based on the theory of the limiting equilibrium method, the safety factor (f_s) of the slope can be obtained
 205 by equilibrium conditions (Zhu et al., 2005). The f_s of the slope can be calculated from Eqs. (14) and (15)
 206 by combining Eqs. (10)-(13) according to the equilibrium condition of force and moment, that is,

$$-\frac{de}{dp}(1 + \tan \psi_\varphi^I \tan \alpha) + \frac{d\chi}{dp}(\tan \psi_\varphi^I - \tan \alpha) = \psi_c^I \sec^2 \alpha + \left(\frac{dw}{dp} + \frac{dv}{dp}\right) \quad (14)$$

$$(\tan \psi_\varphi^I - \tan \alpha) - \frac{dq}{dp}(1 + \tan \psi_\varphi^I \tan \alpha),$$

$$\int_a^b [\lambda f(p)e - e \tan \alpha] dp = \int_a^b \frac{dq}{dp} \Delta s dp. \quad (15)$$

207 3.2. Estimate the safety factor bounds by Bayesian global optimization

208 An essential task of the interval field limit equilibrium method is the propagation of the interval, and
 209 optimization is the most common way to deal with this problem. With the development of optimization
 210 methods, surrogate models have evolved into methods that incorporate new data points based on historical
 211 data and approximate the global optimal solution, i.e., Bayesian global optimization (Jones et al., 1998; Han
 212 and Görtz, 2012). In this paper, we use an improved Bayesian global method to determine the upper and

213 lower bounds of the interval, i.e., the maximum and minimum values (Dang et al., 2022). In this problem,
 214 the optimization problem, including the maximum and minimum values, can be formulated as

$$\left\{ \begin{array}{l} \max f_s(\zeta) \\ \min f_s(\zeta) \\ \text{s.t. } \zeta_j \times \zeta_j = [0, 1], \end{array} \right. \quad (16)$$

215 where $\zeta = (\zeta_1, \zeta_2, \dots, \zeta_l)^\top$ is the l -dimensional vector of interval variables, $f_s(\zeta) : \mathbb{IR}^l \mapsto \mathbb{IR}$ is the objective
 216 function, and $\zeta_j \times \zeta_j = [0, 1]$ is the constraint conditions.

217 Bayesian global optimization is a black-box optimization algorithm for solving optimization problems
 218 for functions with unknown expressions. The algorithm predicts the probability distribution of the function
 219 values at any point based on the function values at a set of sampled points, which is achieved by Gaussian
 220 process regression. In this subsection, a Bayesian global optimization method that can simultaneously find
 221 the minimum and maximum values of the objective function is introduced (Dang et al., 2022). The formula
 222 for calculating the minimum value is exhibited in this section. The maximum value is calculated in a similar
 223 way after the minimum value is obtained. From the results of the Gaussian process regression, an acquisition
 224 function is constructed to measure whether another point is needed to be added, and the extreme value of
 225 the acquisition function is solved to determine the next sampling point. In the paper, Bayesian global
 226 optimization is used to obtain the intervals of f_s .

227 3.2.1. Initial sample selection

228 The first step of the optimization algorithm is to select the initial sample points. In the present imple-
 229 mentation, the initial samples are uniform random samples inside the unit hyper-sphere (Rubinstein and
 230 Kroese, 2016). Then, the initial surrogate model is built based on the initial samples and the associated
 231 function values. The Gaussian process regression $\mathcal{N}[\hat{\gamma}(\zeta), s(\zeta)]$ is used as a surrogate model, in which $\mathcal{N}[\cdot, \cdot]$
 232 is a normal distribution, $\hat{\gamma}(\zeta)$ and $s(\zeta)$ are mean value and standard value of predict model respectively.
 233 It's performed using the fitrgp function in MATLAB.

234 *3.2.2. Training dataset enrichment*

235 For the minimization problem, the objective function improvement $\theta(\zeta)$ is defined as

$$\theta(\zeta) = \max\{\gamma_{\min} - \hat{\gamma}(\zeta), 0\}, \quad (17)$$

236 where γ_{\min} is the current optimal objective function value, and $\hat{\gamma}(\zeta)$ is the set of parameters that obey
237 normal distribution.

238 The expectation value of $\theta(\zeta)$ is given by (Jones et al., 1998)

$$\mathbb{E}[\theta(\zeta)] = \begin{cases} (\gamma_{\min} - \hat{\gamma}(\zeta))\Phi\left(\frac{\gamma_{\min} - \hat{\gamma}(\zeta)}{s(\zeta)}\right) + s(\zeta)\phi\left(\frac{\gamma_{\min} - \hat{\gamma}(\zeta)}{s(\zeta)}\right), & s > 0 \\ 0, & s = 0, \end{cases} \quad (18)$$

239 where $\mathbb{E}[\cdot]$ is the expectation operator, Φ is the standard normal cumulative distribution function, ϕ is
240 the standard normal distribution probability density function, $\hat{\gamma}(\zeta)$ and $s(\zeta)$ are the mean and standard
241 deviation of the normal distribution of the Kriging model predictions, respectively.

242 The new sample points are found by solving the following suboptimization problem which maximize the
243 value of $\mathbb{E}[\theta(\zeta)]$:

$$\begin{cases} \max_{\zeta} \mathbb{E}[\theta(\zeta)] \\ \text{s.t. } \zeta_j \times \zeta_j = [0, 1]. \end{cases} \quad (19)$$

244 *3.2.3. Convergence criterion for Bayesian global optimization*

245 The convergence criterion is an essential element for the optimization algorithm. It is determined by
246 controlling the ratio of the maximum expected value of $\theta(\zeta)$ to the current optimal objective function value.

247 The convergence criterion of the present paper is defined as

$$\frac{|\max \mathbb{E}[\theta(\zeta)]|}{|\gamma_{\min}| + \delta} \leq \epsilon, \quad (20)$$

248 where $\max \mathbb{E}[\theta(\zeta)]$ represents the maximum value of $\mathbb{E}[\theta(\zeta)]$, γ_{\min} represents the minimum value of γ
249 observed so far, δ is an infinitesimal value, ϵ is the threshold value. In this case, δ is 1e-6 and ϵ is 0.001. The
250 optimization process is terminated when the ratio of the maximum expected value of $\theta(\zeta)$ to the current
251 optimal objective function value is less than ϵ for three successive iterations.

252 **4. Implementation procedure of IFLEM**

253 By combining the limit equilibrium method, the interval field model, and Bayesian global optimization
 254 method, IFLEM is proposed to efficiently estimate the upper and lower bounds of the f_s of a slope. The
 255 basic procedure for the numerical implementation of the proposed method (shown in Fig. 3) includes the
 256 following five steps:

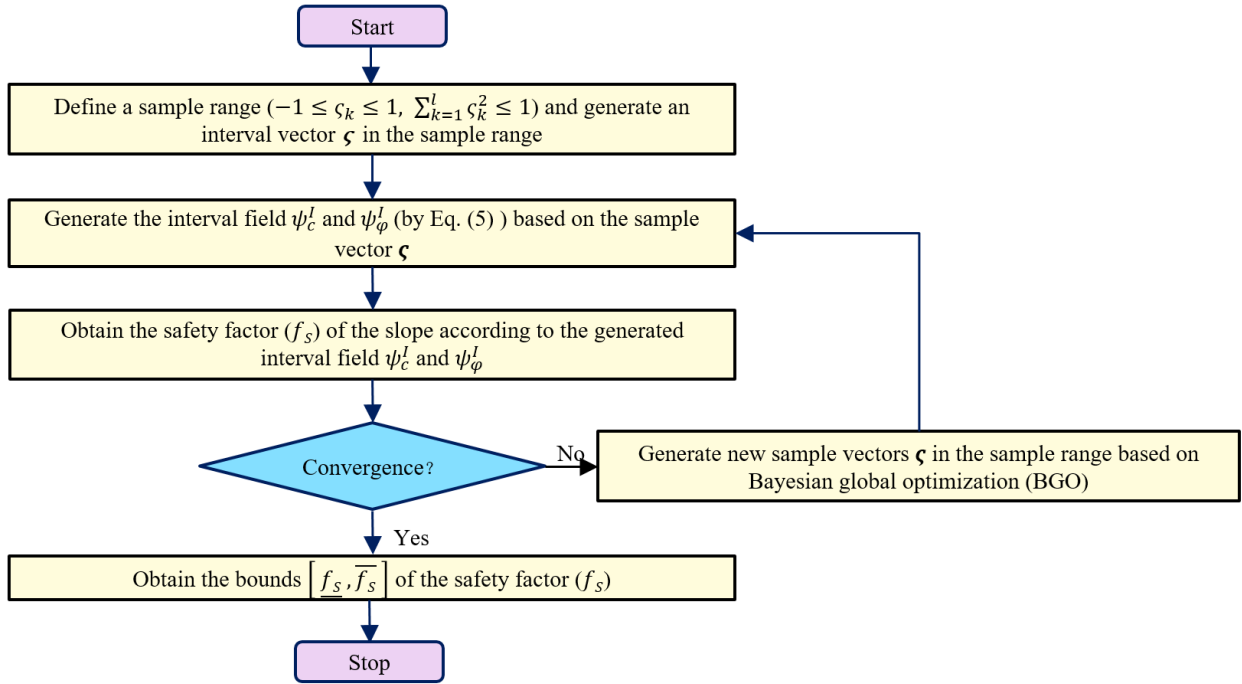


Fig. 3. Flowchart of the proposed IFLEM method

- 257 1. An initial sample points are first generated as a scattering set of samples by the method in Section
 258 3.2. The interval field is generated from Eq. (1) based on the selected interval vector.
- 259 2. The parameters of the interval field are input into the slope model. The f_s of the slope is evaluated
 260 by Eq. (14) according to the interval fields of c and φ .
- 261 3. Select the vector samples required for the next calculation according to the optimal additive point
 262 criterion by Eq. (17).
- 263 4. Determine the termination condition of the optimization by Eq. (20). If the condition is satisfied, the
 264 upper and lower bounds of the f_s are obtained according to the calculation. Otherwise, additional

265 points are required and steps (2) to (4) are repeated until the condition is satisfied.

266 5. After calculating the f_s , the stability of the slope is evaluated. If the minimum value of the f_s is
267 greater than 1, the slope is in a totally safe state. If the maximum value of the f_s is less than 1, the
268 slope is in a high risk state. The stability of the slope is unsure when the interval of the f_s includes
269 1. Within the theoretical framework of interval analysis, there is no information on the probability
270 distribution within the interval. Therefore, the interval field method applied for sparse data cannot
271 obtain the probabilities inside the interval.

272 5. Illustrative examples

273 In order to demonstrate the accuracy and effectiveness of the proposed method, three examples are shown
274 in this section. The first case is a one-stage slope to show the accuracy and efficiency of this approach. The
275 second case is a two-stage to demonstrate the broader applicability of the method. The third case is a
276 real slope to show that this method applies to complex problems and makes the proposed method more
277 meaningful.

278 5.1. Example 1: Interval field analysis of a single-stage slope

279 5.1.1. Description of the problem

280 To illustrate, a single-stage slope is used to demonstrate the generation of the interval field, and then
281 the interval of the f_s is calculated according to the proposed method. This slope has a height of 28 m and
282 an angle of 36.9° , in which the height of the lower floor is 4 m and the height of the upper floor is 24 m,
283 as shown in Fig. 4. In order to generate interval fields for the slope, 489 elements are discrete in the slope.
284 In the process, the c and φ are spatially variable described by the interval fields which are generated by
285 the method mentioned in Section 2. And we use the parameter of midpoint of the element on behalf of the
286 whole element.

287 It is crucial to determine the upper and lower boundaries of the interval field and the parameters of the
288 spatial dependence function when establishing the interval field. This is because interval estimation captures

289 the uncertainty of the parameters through an upper bound with a lower bound. The initial estimation of
 290 interval boundaries can be based on the analyst's expertise and experimental data. However, the expert
 291 knowledge that is available in most practical engineering design cases is sparse, ambiguous, or subjective.
 292 In such cases, it is wise to collect more data to refine the interval. A Bayesian inference scheme can in
 293 this context be used to determine interval bounds on small data sets. It is based on considering a complete
 294 set of parameterized probability density functions to determine the likelihood function, which can then be
 295 used in a Bayesian framework to assess the extreme value distributions on the bounds of the interval, given
 296 the available data. The robustness of the final result is increased by including many possible PDFs in its
 297 computation (Imholz et al., 2020). The parameters of the interval field of the slope are shown in Table 1.
 298 The minimum value of c is 15 kPa and the maximum value is 21 kPa, and the minimum value of φ is 16°
 299 and the maximum value is 24° . The horizontal spatial dependency length l_h is set to 30 m, and the vertical
 300 spatial dependency length l_v is 4 m.

Table 1

Material parameters of the single-stage slope in Example 1

Parameters	Maximum value	Minimum value	l_h	l_v
$c(\text{kPa})$	21	15	30	4
$\varphi(^{\circ})$	24	16	30	4

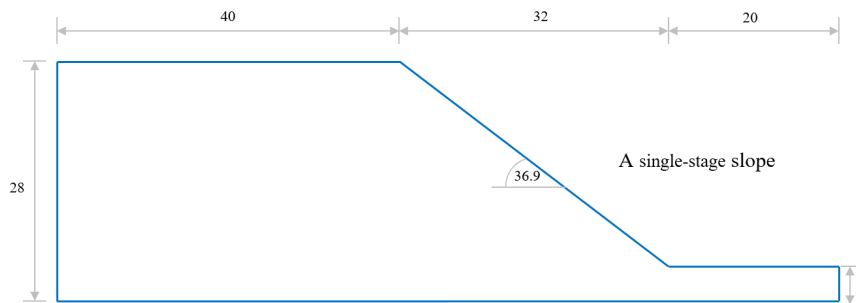


Fig. 4. The geometry model of the single-stage slope

301 5.1.2. Interval field analysis results and discussion

302 First, the interval field of the single-stage slope is generated and the error of the K-L like expansion level
 303 is analyzed. In this example, the error of the K-L like expansion is controlled within 5% and the K-L like
 304 expansion term is six (Huang et al., 2001). Then, the eigenfunctions and eigenvalues are solved according
 305 to the spatial dependency function in Section 2. The eigenfunctions are shown in Fig. 5 and the eigenvalues
 306 are shown in Fig. 6.

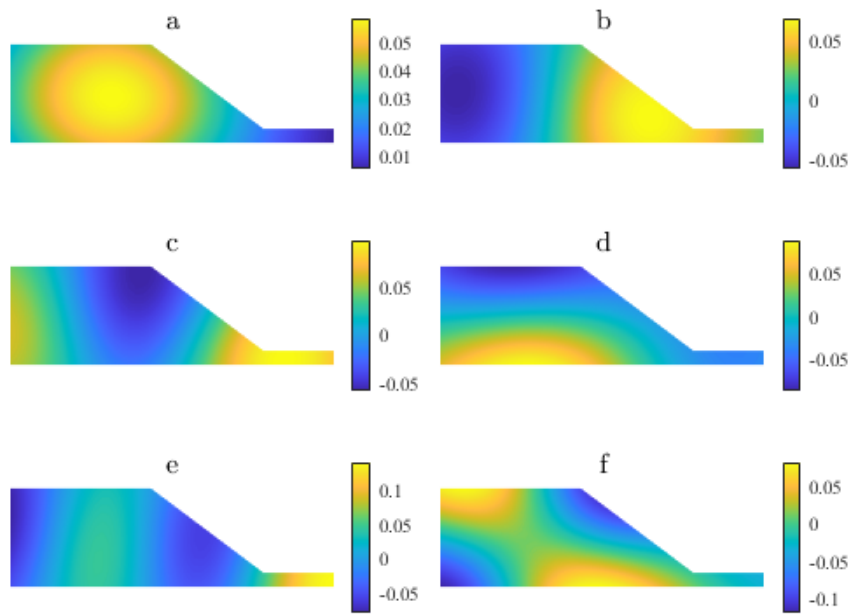


Fig. 5. The first six eigenfunctions of interval fields

307 The single-stage slope with interval field is calculated and its sliding surfaces (SS) are obtained as shown
 308 in Fig. 7. To calculate the f_s , the sliding surfaces should be selected first. For illustration purposes, three
 309 typical sliding surfaces are considered. In this figure, three special sliding surfaces are marked according to
 310 the range of the f_s . The red sliding surface in the diagram represents the most dangerous sliding surface,
 311 while the green sliding surface represents the safest sliding surface. Each sliding surface was analyzed
 312 respectively. The safety factor bounds of the upper and lower of the single-stage slope with interval field
 313 are calculated by the Bayesian global optimization method. The interval of f_s was obtained as [0.83, 0.994]

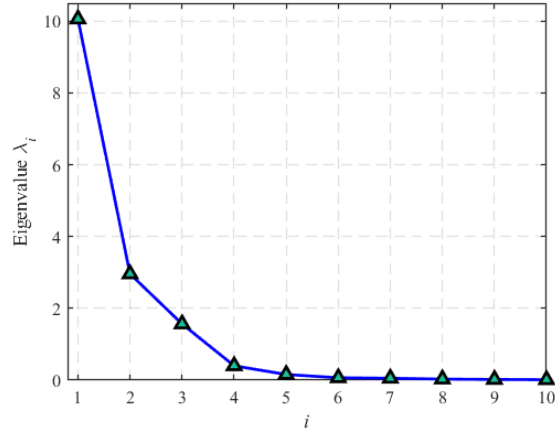


Fig. 6. Eigenvalues of interval fields

314 for the sliding surfaces 1, $[0.946, 1.132]$ for the sliding surfaces 2, and $[1.107, 1.415]$ for the sliding surfaces
 315 3. The calculated interval of f_s is represented in Fig. 8. The optimization of the sliding surface 1 to obtain
 316 the interval of f_s required 19 deterministic analyses, the sliding surface 2 required 20 times, and the sliding
 317 surface 3 required 21 times. In Table 2, the results of the Bayesian global optimization are compared with the
 318 surrogate optimization method. It can be found that Bayesian global optimization shows great advantages
 319 in terms of both computational accuracy and efficiency. For the sliding surface 2 of interval field analysis,
 320 the interval of f_s is $[0.946, 1.132]$. Since $f_s = 1$ is included in the interval of the f_s , the stability of the
 321 slope in this state is unsure, and essentially no fixed statement can be made. This is because there is no
 322 information available on the probability distribution of the c and φ within the bounds of the interval. In
 323 the analysis by the interval method, only the information of the upper and lower boundaries of c and φ
 324 are predicted. Since an interval in essence represents a p-box, bounded by two Heavyside functions, the
 325 probability of obtaining a certain value within the interval is bounded by the interval $[0, 1]$ (Faes and Moens,
 326 2020b), which is completely uninformative. Nonetheless, to be conservative and ensure safety, it is necessary
 327 to increase the lower bound of the f_s though decreasing the angle of the designed slope or enhancing the
 328 slope for this case.

329 For the same c and φ intervals, the interval field with consideration of spatial uncertainty is compared
 330 with the interval analysis method for homogeneous materials. The intervals of f_s were calculated for the

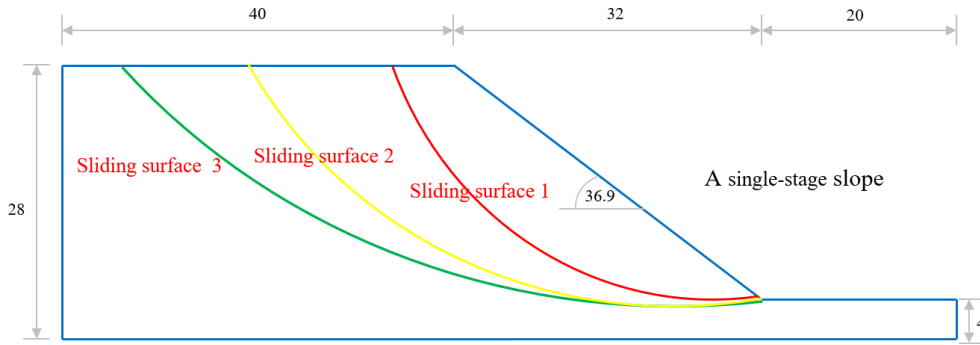


Fig. 7. Three typical sliding surfaces for the single-stage slope failure

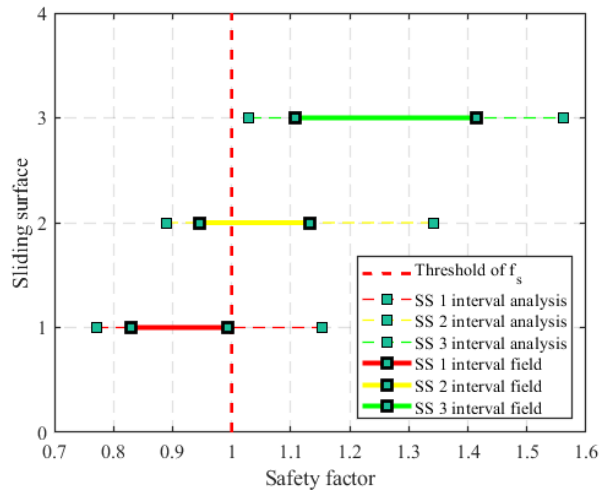


Fig. 8. Results of interval field and interval analysis in the single stage slope analysis

331 interval field and interval analysis, respectively. It can be found in Fig. 8. It can be noticed that the interval
 332 field method can reduce the interval of f_s in comparison with the interval analysis method. Moreover, it is
 333 more consistent with the real situation after considering the spatial uncertainty.

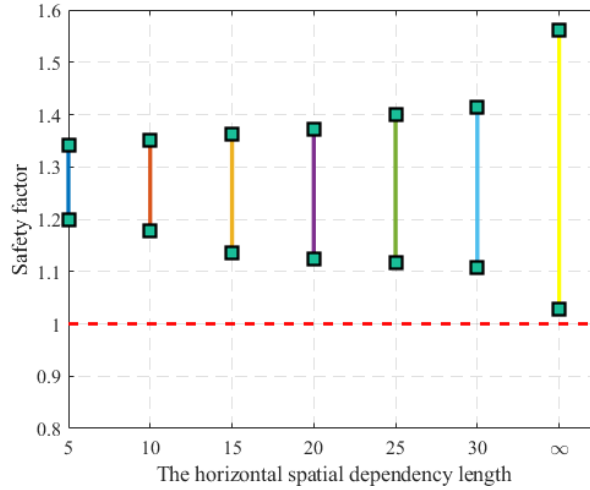
334 In order to study the influence of interval field parameters on the calculation results, the influence of
 335 spatial dependency length on the calculation results of the interval field is analyzed. It's shown in Figs. 9
 336 and 10. The interval fields were calculated for the horizontal spatial dependency lengths of 5 m, 10 m, 15 ,
 337 20 m, 25 m, and 30 m, respectively. The interval fields were calculated for the vertical spatial dependency
 338 lengths of 2 m, 4 m, 6 , 8 m, and 10 m, respectively. When the horizontal spatial dependency length is 5
 339 m, the interval of the calculated results is [1.198, 1.341]. And the interval of the calculated results is [1.107,

Table 2

Results of the efficiency comparison

Method	Result	N
Bayesian optimization	[1.107, 1.415]	21
Surrogate optimization	[1.011, 1.412]	505 + 368

340 1.415] when the horizontal spatial dependency length is 30 m. With the expansion of the input parameter
 341 interval, the interval of the calculated f_s increases rapidly. When the spatial dependency length is greater
 342 than 25m, the percentage of the interval increase of the f_s becomes larger. Therefore, more attention should
 343 be paid to the selection of the spatial dependency length.

**Fig. 9.** Influence of the horizontal spatial dependency length on interval field results

344 In order to explore the influence factors of the interval field, the effect of interval radius is investigated,
 345 as shown in Figs. 11 and 12. Fig. 11 shows the effect of c interval radius on the interval field results, and
 346 Fig. 12 shows the effect of φ interval radius on the interval field results. For the interval radius of c , the
 347 interval field was calculated when it was 1, 2 and 3, respectively. The interval of the calculated results is
 348 [1.127, 1.33] when the c interval radius is 1 kPa. When the radius of the c interval is 3 kPa, the interval
 349 of the calculated results is [1.107, 1.415]. It is noted that when the radius of the c interval increases, the

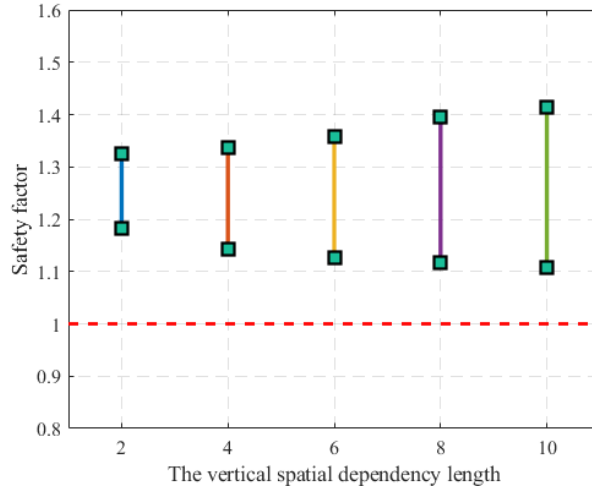


Fig. 10. Influence of the vertical spatial dependency length on interval field results

350 interval of the f_s also increases. However, the percentage of its increase is small. For the interval radius
 351 of φ , the interval field was calculated for its 1, 2, 3, and 4, respectively. When the φ interval radius is 1° ,
 352 the calculated interval is [1.215, 1.314]. And the interval of the calculated results is [1.107, 1.415] when the
 353 radius of the φ interval is 4° . It can be seen that when the radius of the φ interval increases, the interval
 354 of the f_s also increases. And the percentage of its increase is larger than the radius of the c interval. It
 355 indicates that the φ interval radius has a greater effect on the interval results of the f_s than the c interval
 356 radius. Therefore, it can be seen that more attention should be paid to the selection interval radius of the
 357 φ . More detailed results can be obtained using interval sensitivity analysis (Moens and Vandepitte, 2007).

358 5.2. Example 2: Interval field analysis of a two-stage slope

359 5.2.1. Description of the problem

360 For illustration, a two-stage slope is used to demonstrate the generation of the interval field, and then
 361 the interval of f_s is calculated according to the proposed method. This slope has a lower layer height of 10
 362 m and an upper layer height of 19 m, as shown in Fig. 13. The height of the first slope is 9 m and the angle
 363 is 42° . The height of the second slope is 10 m and the angle is 40° . The c interval of the lower layer is [4,
 364 6], the φ interval is [28, 30], and the spatial dependency length is 5 m. The c interval of the upper layer is

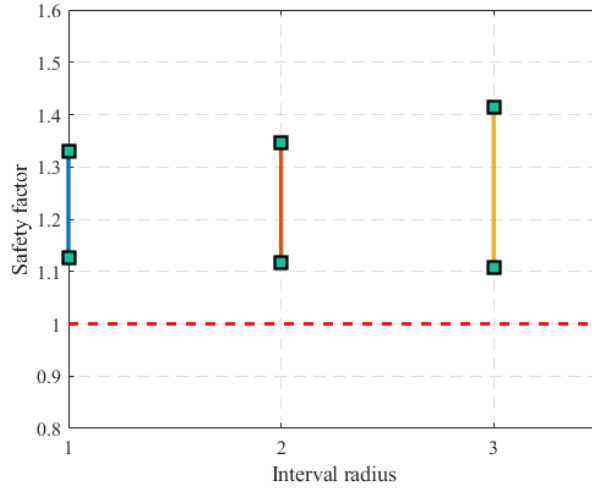


Fig. 11. Influence of cohesive interval radius on interval field results

365 [10, 12], the φ interval is [28, 36], and both horizontal and vertical spatial dependency lengths are both 5
 366 m. The material parameters are shown in Table 3.

Table 3

Material parameters of the two-stage slope in Example 2

Layers	c (kPa)	φ ($^{\circ}$)	l_h	l_v
Lower level	[4, 6]	[24, 26]	5	5
Upper level	[6, 10]	[24, 30]	5	5

367 5.2.2. Interval field analysis results

368 First, the interval field of the two-stage slope is generated, as shown in Fig. 14. This figure is a one-time
 369 realization of the sample values of the interval field. For this two-stage slope, the generated interval fields
 370 are calculated separately for the upper and lower layers. The two-stage slope with interval field is calculated
 371 and its slip surface is obtained as shown in Fig. 15. In this figure, three special sliding surfaces are marked.
 372 Each type of sliding surface represents a typical picture of the minimum f_s in that region. And each sliding
 373 surfaces is analyzed. The interval of f_s was obtained as [1.113, 1.440] for the sliding surface 1, [1.069, 1.117]
 374 for the sliding surface 2, and [1.505, 1.529] for the sliding surface 3. The calculated interval of the f_s is

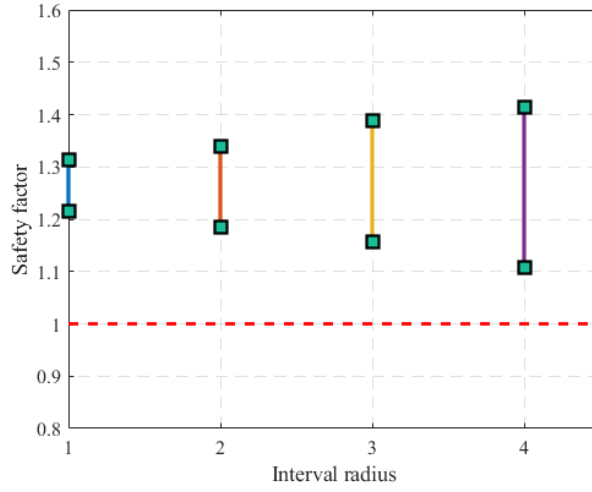


Fig. 12. Influence of the interval radius of the φ on the interval field results

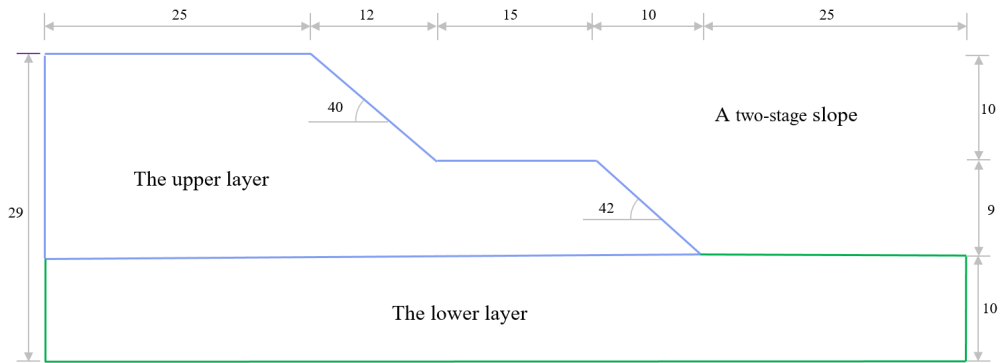


Fig. 13. The geometry model of the two-stage slope

375 represented in Fig. 16.

376 The intervals of f_s were calculated for the interval field and interval analysis, respectively. The results
 377 of the interval limit equilibrium method are compared with those of the interval field limit equilibrium
 378 method, as shown in Table 4. It can be noticed that the interval field method can reduce the interval of
 379 f_s in comparison with the interval analysis method. And it is obvious that the result of the interval field
 380 is larger than 1 so the slope is safe definitely. But the interval analysis lower bound of the f_s at sliding
 381 surfaces 1 and 2 is less than 1 down to it is unsure in safety state. From this it can be seen that the result of
 382 the interval analysis method is more conservative. However, the result of the interval field method is more

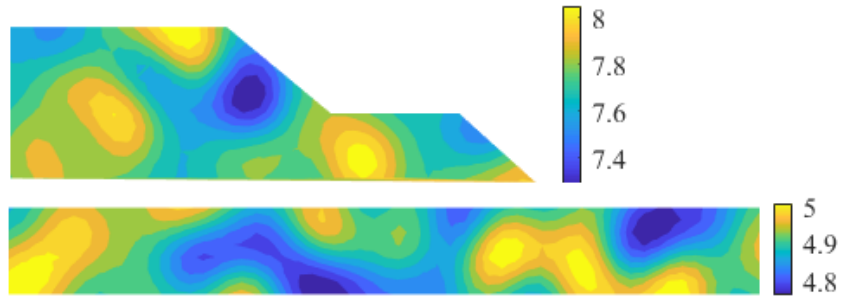


Fig. 14. Sample values realization for the interval field of the two-stage slope

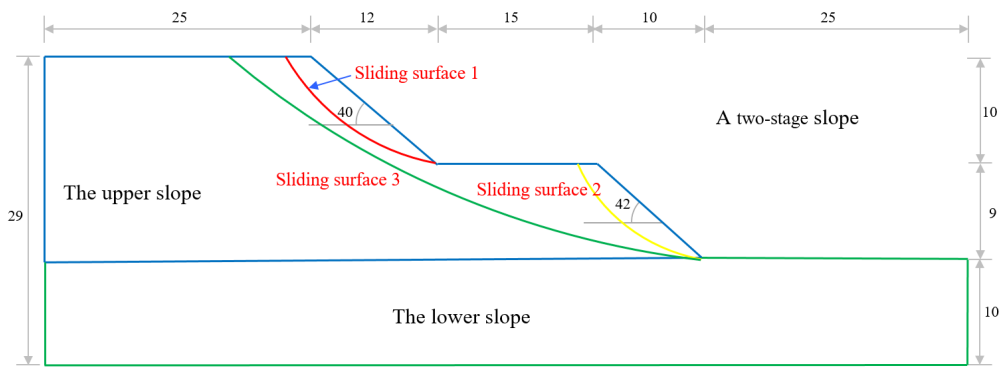


Fig. 15. Three typical sliding surfaces for the two-stage slope failure

383 realistic since it can reflect the spatial uncertainty.

Table 4

Results of interval field in the two-stage slope analysis

Type	Sliding surface 1	Sliding surface 2	Sliding surface 3
Interval field	[1.113, 1.140]	[1.069, 1.117]	[1.505, 1.529]
Interval analysis	[0.953, 1.342]	[0.939, 1.306]	[1.291, 1.719]

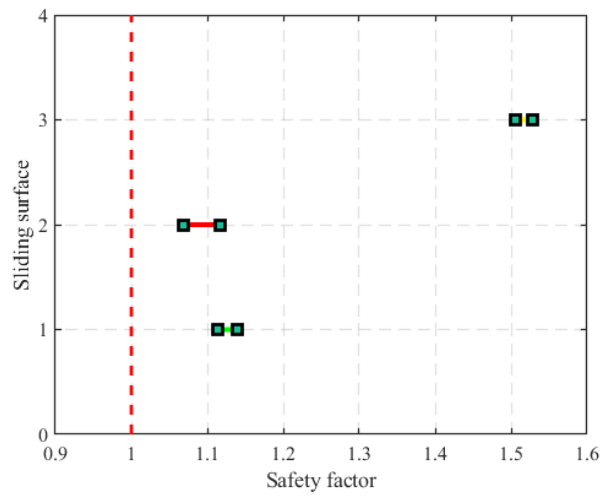


Fig. 16. Results of interval field in the two-stage slope analysis

384 5.3. Example 3: Interval field analysis of the Majiagou landslide

385 5.3.1. Description of the Majiagou landslide

386 The Majiagou landslide is on the left bank of the Zhaxi River, a tributary of the Yangtze River in
387 Zigui County, Hubei Province, as shown in Fig. 17 (a) (Zhang et al., 2021). According to the field survey,
388 the Majiagou landslide is a slope with an east-west distribution of alternating gentle and steep with an
389 average slope of 15° . The landslide extends 538 m horizontally, of which the elevation of the toe of the
390 slope is 135 m, and the elevation of the crown is 280 m. The geometric model is shown in Fig. 17 (b).
391 The Majiagou landslide is mainly composed of surface deposits and sedimentary bedrock. The sedimentary
392 bedrock consists of Jurassic Suining Formation grey sandstone interbedded with purple-red mudstone. The
393 surface deposits are mainly composed of silty clay mixed with gravelly soil. The silty mudstone is easily
394 softened and highly fractured and is one of the most common slip-prone strata in the Three Gorges reservoir
395 area. The soil-rock interface composed of weathered silty mudstone was identified as the main sliding surface
396 combining geological investigation and drilling technology (Liao et al., 2021). Table. 5 lists the properties
397 of the landslide material (Ma et al., 2017).

Table 5

Material parameters of the real-slope in Example 3

Materials	Unit weight(kN/m ³)	c (kPa)	φ ($^\circ$)	l_h (m)	l_v (m)
Sliding mass	21.14	[13, 23]	[15, 23]	50	10
Sliding zone	19.40	[13, 23]	[13, 21]	50	10

398 5.3.2. Interval field analysis results

399 First, the interval field of the Majiagou landslide is generated. In this process, the interval field is
400 established separately in two parts: the sliding zone and the sliding mass. The error in the interval field
401 discretisation remains within 5%. Then, the generated interval field parameters of c and φ are assigned
402 to the numerical model of the Majiagou landslide. A deterministic analysis of this Majiagou landslide is
403 performed according to the interval field limit equilibrium method formula. Finally, the interval of the f_s of

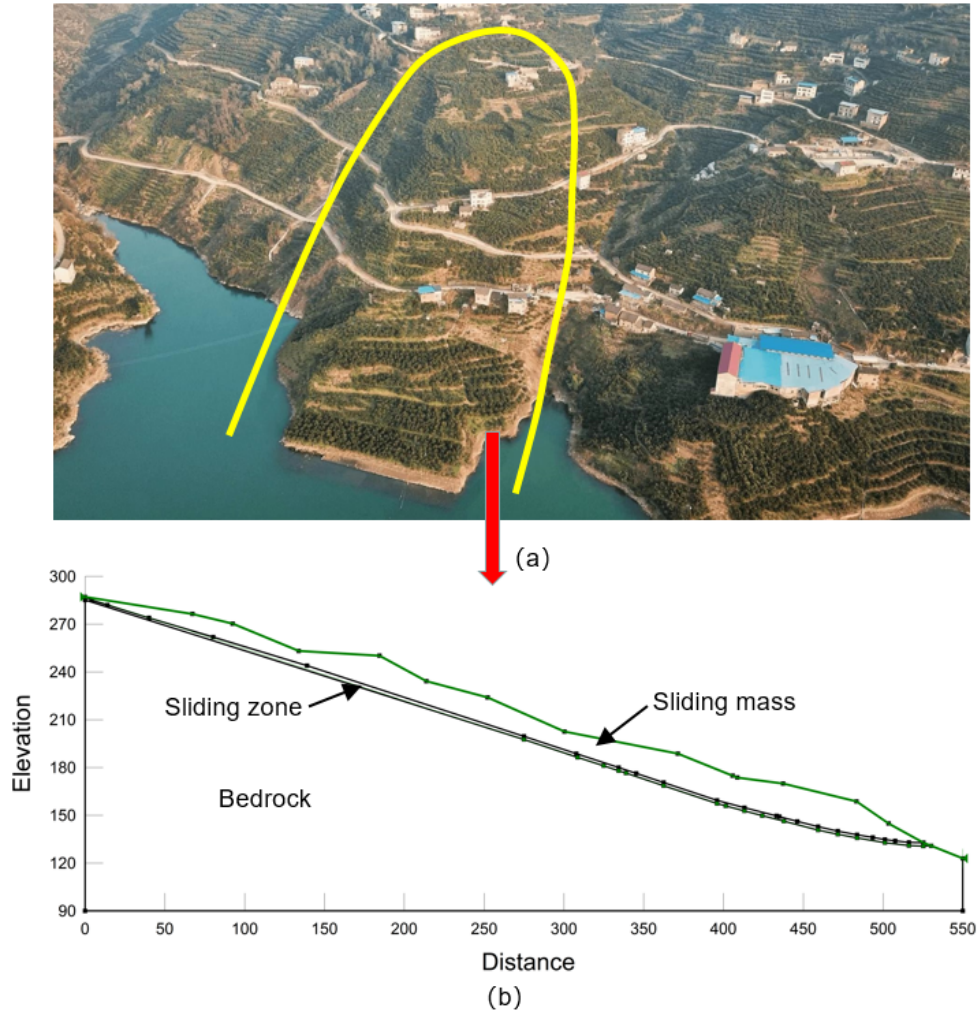


Fig. 17. The geometry model of the Majiagou landslide

404 the Majiagou landslide is calculated using the Bayesian global optimization method. The interval of f_s was
 405 obtained as [1.186, 1.215] for the determined sliding surface. The propagation of the interval field requires
 406 only 22 deterministic calculations. This shows the high applicability of the method for complex problems.
 407 Then, the effect of Bayesian global optimization initial points on the results of f_s intervals is investigated.
 408 The Bayesian global optimization was performed 20 times for the Majiagou landslide with an interval field,
 409 based on different starting points. Based on these 20 runs, the variance of the interval's maximum and
 410 minimum values is assessed to estimate the robustness of the method with respect to the selection of the
 411 initial points. The variance of the maximum and minimum values was obtained as 1.085e-5 and 3.654e-6,

412 respectively. The f_s results are very stable, indicating the method's robustness.

413 6. Concluding remarks

414 The main contribution of this work is the proposal of a new interval field limit equilibrium method,
415 IFLEM, for efficiently estimating the interval of the f_s of a slope in the presence of spatial uncertainty.
416 For our purpose, the IFLEM method first characterizes the interval field by using the Karhunen-Loève
417 like expansion. Further, based on the Morgenstern-Price method and the generated interval field (IF),
418 a computational method for calculating the f_s of slopes is proposed. Then, to efficiently and accurately
419 solve the optimization problem for the upper and lower bounds of the f_s , a dedicated iterative algorithm
420 is developed based on Bayesian global optimization (BGO). Finally, the IFLEM is formed by an elegant
421 combination of IF and LEM. The main feature of IFLEM is the ability to obtain the interval of the f_s ,
422 resulting from uncertainties in model parameters and their spatial uncertainty. Three numerical examples
423 are presented to illustrate the availability and effectiveness of the proposed approach. The main concluding
424 remarks includes:

- 425 1. The numerical results indicate that the proposed method allows to perform the uncertainty analysis of
426 slopes in the presence of sparse data. Noting that the upper and lower bounds of the f_s are obtained
427 with a small number of deterministic analyses, the proposed method seems to be effective and efficient
428 for quantitative analysis of slopes with scarce data.
- 429 2. The influences of the spatial dependency length and the interval radius are investigated. The results
430 shows that different values of spatial dependency length can result in a large variation of the interval
431 of f_s . Besides, compared to the interval radius of c , the interval of f_s is more sensitive to the interval
432 radius of φ . Hence, it is of great significance to reasonably determine the spatial dependency length
433 and the interval radius of φ in the interval field analysis of slopes.
- 434 3. The comparison between interval field analysis and interval analysis with homogeneous materials is
435 also performed. Evident differences are observed in the results of the two methods, which implies that

436 the consideration of spatial uncertainty is necessary in the uncertainty quantification of geotechnical
437 engineering structures.

438 4. Since the deterministic analysis participate the interval field analysis in a decoupled manner, any
439 existing solvers can be easily incorporated into the computational procedure, which makes the method
440 quite general.

441 5. Due to the high efficiency and generality of the IFLEM, it shows a great potential for the uncertainty
442 quantification of large-scale problems with complicated boundary conditions or practical engineering
443 problems in real world.

444 Despite the encouraging results of the present study, many further works need to be carried out. In
445 the follow-up study, it is hoped that some advanced slope analysis methods can be incorporated into the
446 proposed method. The consideration of interval reliability analysis methods and interval field expansion
447 methods is another future research effort.

448 **Declaration of competing interest**

449 The authors declare that they have no known competing financial interests or personal relationships that
450 could have appeared to influence the work reported in this paper.

451 **Acknowledgement**

452 This work is supported by the China Scholarship Council (CSC). Chengxin Feng, Chao Dang and Jiashu
453 Yang has received financial support from China Scholarship Council (CSC). Zhibao Zheng is grateful to the
454 Alexander von Humboldt Foundation.

455 **References**

- 456 Atkinson, K., Han, W., 2009. Numerical solution of fredholm integral equations of the second kind, in: Theoretical Numerical
457 Analysis. Springer, pp. 473–549.
- 458 Beer, M., Zhang, Y., Quek, S.T., Phoon, K.K., 2013. Reliability analysis with scarce information: Comparing alternative
459 approaches in a geotechnical engineering context. *Structural Safety* 41, 1–10.

460 Callens, R.R.P., Faes, M.G.R., Moens, D., 2021. Local explicit interval fields for non-stationary uncertainty modelling in finite
461 element models. *Computer Methods in Applied Mechanics and Engineering* 379, 113735.

462 Cami, B., Javankhoshdel, S., Phoon, K.K., Ching, J., 2020. Scale of Fluctuation for Spatially Varying Soils: Estimation
463 Methods and Values. *ASCE-ASME Journal of Risk and Uncertainty in Engineering Systems, Part A: Civil Engineering* 6,
464 03120002.

465 Catalo, L., 2004. Genetic anti-optimization for reliability structural assessment of precast concrete structures. *Computers &
466 Structures* 82, 1053–1065.

467 Chen, Z.Y., Imholz, M., Li, L., Faes, M., Moens, D., 2020. Transient landing dynamics analysis for a lunar lander with random
468 and interval fields. *Applied Mathematical Modelling* 88, 827–851.

469 Dang, C., Wei, P., Faes, M.G., Valdebenito, M.A., Beer, M., 2022. Interval uncertainty propagation by a parallel Bayesian
470 global optimization method. *Applied Mathematical Modelling* 108, 220–235.

471 Deng, Z., Guo, Z., Zhang, X., 2017. Interval model updating using perturbation method and radial basis function neural
472 networks. *Mechanical Systems and Signal Processing* 84, 699–716.

473 Elishakoff, I., Cai, G., Starnes Jr, J., 1994. Non-linear buckling of a column with initial imperfection via stochastic and
474 non-stochastic convex models. *International Journal of Non-Linear Mechanics* 29, 71–82.

475 Faes, M., Moens, D., 2017. Identification and quantification of spatial interval uncertainty in numerical models. *Computers &
476 Structures* 192, 16–33.

477 Faes, M., Moens, D., 2019. Multivariate dependent interval finite element analysis via convex hull pair constructions and the
478 Extended Transformation Method. *Computer Methods in Applied Mechanics and Engineering* 347, 85–102.

479 Faes, M., Moens, D., 2020a. On auto- and cross-interdependence in interval field finite element analysis. *International Journal
480 for Numerical Methods in Engineering* 121, 2033–2050.

481 Faes, M., Moens, D., 2020b. Recent trends in the modeling and quantification of non-probabilistic uncertainty. *Archives of
482 Computational Methods in Engineering* 27, 633–671.

483 Faes, M.G., Broggi, M., Spanos, P.D., Beer, M., 2022. Elucidating appealing features of differentiable auto-correlation functions:
484 A study on the modified exponential kernel. *Probabilistic Engineering Mechanics* , 103269.

485 Griffiths, D.V., Fenton, G.A., 2004. Probabilistic Slope Stability Analysis by Finite Elements. *Journal of Geotechnical and
486 Geoenvironmental Engineering* 130, 507–518.

487 Han, Z.H., Görtz, S., 2012. Hierarchical Kriging Model for Variable-Fidelity Surrogate Modeling. *AIAA Journal* 50, 1885–1896.
488 Publisher: American Institute of Aeronautics and Astronautics.

489 Huang, S., Quek, S., Phoon, K., 2001. Convergence study of the truncated Karhunen-Loève expansion for simulation of
490 stochastic processes. *International Journal for Numerical Methods in Engineering* 52, 1029–1043.

491 Imholz, M., Faes, M., Vandepitte, D., Moens, D., 2020. Robust uncertainty quantification in structural dynamics under scarce
492 experimental modal data: A bayesian-interval approach. *Journal of Sound and Vibration* 467, 114983.

493 Jiang, S.H., Huang, J., Griffiths, D., Deng, Z.P., 2022. Advances in reliability and risk analyses of slopes in spatially variable
494 soils: A state-of-the-art review. *Computers and Geotechnics* 141, 104498.

495 Jones, D.R., Schonlau, M., Welch, W.J., 1998. Efficient Global Optimization of Expensive Black-Box Functions. *Journal of*
496 *Global Optimization* 13, 455–492.

497 Liao, K., Wu, Y., Miao, F., Li, L., Xue, Y., 2021. Time-varying reliability analysis of majiagou landslide based on weakening
498 of hydro-fluctuation belt under wetting-drying cycles. *Landslides* 18, 267–280.

499 Liu, S., Shao, L., Li, H., 2015. Slope stability analysis using the limit equilibrium method and two finite element methods.
500 *Computers and Geotechnics* 63, 291–298.

501 Lämsivaara, T., Phoon, K.K., Ching, J., 2021. What is a characteristic value for soils? *Georisk: Assessment and Management*
502 *of Risk for Engineered Systems and Geohazards* , 1–26.

503 Ma, J., Tang, H., Hu, X., Bobet, A., Zhang, M., Zhu, T., Song, Y., Ez Eldin, M.A., 2017. Identification of causal factors for
504 the majiagou landslide using modern data mining methods. *Landslides* 14, 311–322.

505 Moens, D., De Munck, M., Desmet, W., Vandepitte, D., 2011. Numerical dynamic analysis of uncertain mechanical structures
506 based on interval fields, in: *IUTAM symposium on the vibration analysis of structures with uncertainties*, Springer. pp.
507 71–83.

508 Moens, D., Hanss, M., 2011. Non-probabilistic finite element analysis for parametric uncertainty treatment in applied mechanics:
509 Recent advances. *Finite Elements in Analysis and Design* 47, 4–16.

510 Moens, D., Vandepitte, D., 2007. Interval sensitivity theory and its application to frequency response envelope analysis of
511 uncertain structures. *Computer Methods in Applied Mechanics and Engineering* 196, 2486–2496.

512 Montoya-Noguera, S., Zhao, T., Hu, Y., Wang, Y., Phoon, K.K., 2019. Simulation of non-stationary non-Gaussian random
513 fields from sparse measurements using Bayesian compressive sampling and Karhunen-Loève expansion. *Structural Safety* 79,
514 66–79.

515 Morgenstern, N.u., Price, V.E., 1965. The analysis of the stability of general slip surfaces. *Geotechnique* 15, 79–93.

516 Ni, B.Y., Jiang, C., 2020. Interval field model and interval finite element analysis. *Computer Methods in Applied Mechanics*
517 *and Engineering* 360, 112713.

518 Phoon, K.K., Kulhawy, F.H., 1999a. Characterization of geotechnical variability. *Canadian Geotechnical Journal* 36, 612–624.
519 Publisher: NRC Research Press.

520 Phoon, K.K., Kulhawy, F.H., 1999b. Evaluation of geotechnical property variability. *Canadian Geotechnical Journal* 36,
521 625–639.

522 Rubinstein, R.Y., Kroese, D.P., 2016. *Simulation and the Monte Carlo method*. John Wiley & Sons.

523 Sofi, A., 2015. Structural response variability under spatially dependent uncertainty: stochastic versus interval model. *Proba-*
524 *bilistic Engineering Mechanics* 42, 78–86.

525 Sofi, A., Muscolino, G., Elishakoff, I., 2015. Static response bounds of Timoshenko beams with spatially varying interval

526 uncertainties. *Acta Mechanica* 226, 3737–3748.

527 Sofi, A., Romeo, E., Barrera, O., Cocks, A., 2019. An interval finite element method for the analysis of structures with spatially
528 varying uncertainties. *Advances in Engineering Software* 128, 1–19.

529 Spanos, P.D., Beer, M., Red-Horse, J., 2007. Karhunen-Loève expansion of stochastic processes with a modified exponential
530 covariance kernel. *Journal of Engineering Mechanics* 133, 773–779.

531 Wang, C., Qiu, Z., Wang, X., Wu, D., 2014. Interval finite element analysis and reliability-based optimization of coupled
532 structural-acoustic system with uncertain parameters. *Finite Elements in Analysis and Design* 91, 108–114.

533 Wang, Y., Zhao, T., Phoon, K.K., 2019. Statistical inference of random field auto-correlation structure from multiple sets of
534 incomplete and sparse measurements using Bayesian compressive sampling-based bootstrapping. *Mechanical Systems and*
535 *Signal Processing* 124, 217–236.

536 Zhang, L., Shi, B., Zhu, H., Yu, X.B., Han, H., Fan, X., 2021. Pso-svm-based deep displacement prediction of majiagou
537 landslide considering the deformation hysteresis effect. *Landslides* 18, 179–193.

538 Zhu, D.Y., Lee, C.F., Qian, Q.H., Chen, G.R., 2005. A concise algorithm for computing the factor of safety using the
539 morgenstern-price method. *Canadian Geotechnical Journal* 42, 272–278.